Journal of Animal Science, 2026, **104**, skag134
https://doi.org/10.1093/jas/skag134
Published: 9 May 2026
Reproduction

Stage-specific remodeling of wingless-related integration sites (WNT) signaling during oocyte-to-embryo transition in pigs

Carolina G. Cabrera-Gomez[1,2], David Gascon-Collado[1,2], Paula Blanco-Cueto[1], Belen Pequeño[1], Heriberto Rodriguez-Martinez[3], and Cristina A. Martinez-Serrano*[,1,3],

[1]Department of Biotechnology, National Institute for Agriculture and Food Research and Technology (INIA-CSIC), Madrid, 28040, Spain
[2]Faculty of Veterinary Sciences, Universidad Complutense de Madrid (UCM), Campus de Ciudad Universitaria, Madrid, 28040, Spain
[3]Department of Biomedical & Clinical Sciences (BKV), BKH/Obstetrics & Gynecology, Faculty of Medicine and Health Sciences, Linköping University, Linköping, SE-58185, Sweden
*Corresponding author. Email: cristina.martinez@inia.csic.es

Abstract

The WNT signaling pathway is a central regulator of cell polarity, adhesion, cytoskeletal dynamics, and lineage specification during early embryonic development. Although its roles have been extensively studied in murine and human models, the temporal regulation and pathway architecture of WNT signaling during early porcine development remain poorly defined. Here, we performed a comprehensive transcriptomic analysis to characterize WNT pathway dynamics across key stages of pig in vitro development, including immature oocytes (IMO), mature oocytes (MO), zygotes (ZY), cleaved embryos (2–4 cells; CL), and blastocysts (BL). Global analyses revealed major transcriptomic transitions (FDR <0.05; $|\text{Fold Change}| \geq 2$) during oocyte maturation and blastocyst formation, whereas zygotes and cleaved embryos exhibited highly similar expression profiles. Module-based and gene-level analyses showed that oocyte maturation is associated with increased expression of extracellular WNT antagonists and components of the β-catenin destruction complex, together with selective regulation of Frizzled receptors, consistent with tight control of canonical WNT signaling at the MII stage. Following fertilization, this inhibitory configuration was partially relieved, alongside transient upregulation of specific WNT ligands, transcriptional mediators, and adhesion-related components during zygotic genome activation and early cleavage. At the blastocyst stage, WNT signaling became increasingly associated with planar cell polarity and epithelial organization modules. Together, the data reveal a highly dynamic and stage-specific restructuring of WNT signaling during early porcine development. Our findings indicate that precise temporal modulation—rather than uniform activation—of WNT pathway components accompanies the porcine oocyte-to-embryo transition, providing a molecular framework to better understand early developmental regulation and offering insights relevant to reproductive biotechnology and developmental biology.

Lay Summary

Early development depends on precise communication between cells, guided by molecular signaling pathways. One of these pathways, known as WNT signaling, plays a key role in shaping cells, controlling their interactions, and guiding early embryonic organization. While WNT signaling has been well studied in some model species, much less is known about how it operates during early development in pigs. In this study, we analyzed how genes involved in WNT signaling change their activity during key stages of porcine development, from immature and mature egg cells (oocytes) through fertilized eggs (zygotes) to the blastocyst stage. Using RNA sequencing, we found that WNT-related genes regulated in a stage-specific manner. Our results show that WNT signaling is strongly restrained as the egg cell completes maturation, likely to prevent inappropriate gene activation before fertilization. Then, this restraint is partially lifted, allowing the early embryo to re-engage WNT signaling as it begins to activate its own genome. At later stages, WNT signaling becomes increasingly linked to cell structure and tissue organization during blastocyst formation. These findings provide new insight into how early porcine development is regulated at the molecular level and help explain why timing of signaling pathways is essential for successful embryo development.

Received: January 26, 2026. **Accepted:** April 7, 2026

Keywords embryo, oocyte, porcine, WNT pathway

Abbreviations: APC, adenomatous polyposis coli; ART, assisted reproductive technologies; BL, blastocysts; BSA, bovine serum albumin; CK1, casein kinase 1; CL, cleaved embryos; COC, cumulus-oocyte complexes; CTNNB1, catenin beta 1; CTNND1, catenin delta-1; DEG, differentially expressed genes; DICE, database of immune cell expression; DKK, Dickkopf Wnt Signaling Pathway Inhibitor; dPBS, Dulbecco's phosphate-buffered solution; eCG, equine chorionic gonadotropin; ET, embryo transfer; FDR, false discovery rate; FRZ, frizzled; FRZB, FRZ-related protein; GSK3, glycogen synthase kinase 3; hCG, human chorionic gonadotropin; IMO, immature oocytes; IVC, in vitro culture; IVF, in vitro fertilization; IVM, in vitro maturation; IVP, in vitro production; KEGG, Kyoto encyclopedia of genes and genomes; LEF, lymphoid enhancer-binding factor; LRG4, leucine-rich repeat–containing G protein-coupled receptor 4; LRP, low density lipoprotein receptor protein; MAPK, mitogen-activated protein kinases; MO, mature oocytes; NCSU-23, North Carolina State University 23; PCA, principal component analysis; RNA, ribonucleic acid; RNA-seq, RNA-sequencing; SFRP3, secreted FRZ-related protein 3; TCF, T-cell factor; TCM-199, tissue Culture Medium 199; TL-HEPES-PVA, Tyrode's lactate-HEPES-polyvinyl alcohol; WNT, wingless-related mouse mammary tumor viruses; ZP, zona pellucida; ZY, zygotes

Graphical abstract

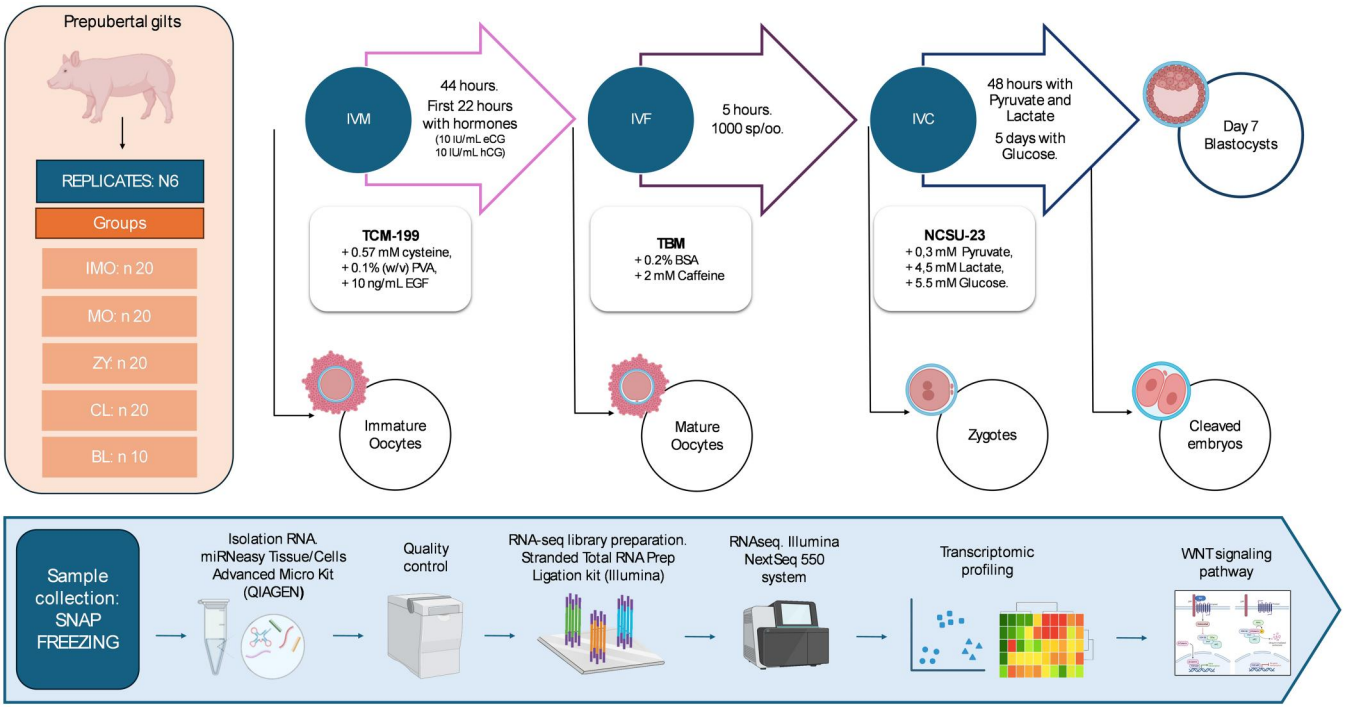

Introduction

In mammals, the acquisition of oocyte competence and the regulation of early embryonic events are tightly coordinated processes that determine developmental potential and reproductive success (Fuentes et al 2024). Understanding these processes is essential not only for advancing basic developmental biology but also for improving assisted reproductive technologies (ART) and reproductive efficiency in livestock species (Martinez et al 2019; Domínguez-Oliva et al 2023; Hamze et al 2025). The pig is particularly relevant in this context, both as a major source of animal protein and as a valuable biomedical model due to its physiological and genomic similarities to humans (Lin-Schilstra et al 2022). Therefore, elucidating the molecular mechanisms underlying porcine oocyte and early embryo development has important implications for both animal production and translational research.

In this framework, studying the molecular mechanisms that regulate the transition from oocyte to embryo is of particular interest. The wingless-related mouse mammary tumor viruses (WNT) signaling pathway is a key developmental regulator, orchestrating cell polarity, adhesion, cytoskeletal remodeling, proliferation, and lineage specification across mammalian embryogenesis (Nusse and Clevers 2017; Steinhart and Angers 2018). In oocytes and preimplantation embryos, WNT influences meiotic competence, spindle positioning, cytoplasmic maturation, fertilization readiness, zygotic genome activation, and the emergence of trophectoderm-inner cell mass identities (Tribulo et al 2017). While these roles have been extensively characterized in murine and human models, the temporal dynamics, ligand-receptor usage, and canonical vs non-canonical balance remain poorly defined in the porcine species. This represents a critical knowledge gap, as pigs exhibit species-specific reproductive features (prolonged embryonic genome activation, delayed compaction, and distinct cell fate allocation) that make them both an agricultural priority and a valuable biomedical model (Bazer and Johnson 2014; Hamze et al 2025). Moreover, improving in vitro embryo production efficiency in pigs requires understanding molecular pathways, such as WNT, if regulating oocyte

competence and early developmental progression. Despite evidence that WNT modulators affect porcine oocyte maturation, cumulus expansion, and blastocyst formation (Huang et al 2013; Liu et al 2020), a systematic transcriptomic characterization of WNT-pathway dynamics across the oocyte-to-embryo transition is yet lacking. Therefore, elucidating how WNT signaling is regulated during early porcine development seems essential to gain deeper insights into developmental biology pre-requisites to advance reproductive biotechnology and translational applications.

The present study aimed therefore to characterize gene expression profiles across the main stages of pig embryo development: immature and mature oocytes, zygotes, early cleavage-stage embryos (2–4 cells), and blastocysts. This integrative approach provides a comprehensive view of the transcriptional changes that accompany developmental progression and may help identify molecular signatures associated with oocyte and embryo quality and viability.

Materials and methods

Experimental design

We profiled gene expression across five developmental stages in the porcine species: immature oocytes (IMO), mature oocytes (MO), zygotes (ZY), cleaved embryos (CL), and blastocysts (BL). For each stage, we generated six biological replicates, each replicate consisting of a pool of 20 IMO, MO, ZY, or CL or 10 BL collected across independent donor batches. The experimental unit was the biological replicate (pooled sample). Total ribonucleic acid (RNA) was extracted from samples and analyzed by RNA-sequencing (RNA-seq) to identify differentially expressed genes (DEG) among groups.

Chemicals

All chemicals used were obtained from the Merk Sigma-Aldrich Chemical Company (Madrid, Spain) unless specified otherwise.

Embryo in vitro production (IVP)

Collection of cumulus-oocyte complexes (COC)

Offal ovaries were collected from prepubertal crossbred gilts slaughtered at a commercial slaughterhouse (Comarán, S.L. Aranjuez, Madrid). Immediately after collection, the ovaries were shipped to our laboratory in 0.9 mg/mL NaCl containing kanamycin (70 µg/mL) at 33 °C. Medium-sized follicles (3–7 mm in diameter) were cut with a sterile scalpel blade in Tyrode's lactate-HEPES-polyvinyl alcohol (TL-HEPES-PVA). Only the COC containing two or more layers of compact cumulus cells were selected for this experiment.

In vitro maturation (IVM)

Groups of 70–75 COC were washed and cultured in a four-well multi-dish (Nunc, Roskilde, Denmark) containing 500 μL of maturation medium (Tissue Culture Medium 199 [TCM-199]) supplemented with 0.55 mM glucose, 0.9 mM sodium pyruvate, 75 µg/mL penicillin, 50 µg/mL streptomycin, 1 mg/mL PVA, 0.57 mM cysteine, and 10 ng/mL epidermal growth factor. IVM medium was also supplemented with 10 IU/mL equine chorionic gonadotropin (eCG) (Folligon, Intervet International B.V. Boxmeer, The Netherlands) and 10 IU/mL human chorionic gonadotropin (hCG) (Veterin corion, Divasa Farmavic S.A. Barcelona, Spain) for the first 22 h of IVM. The COC were then incubated for an additional 22 h in the same medium without hormones. All steps were performed under paraffin oil at 38 °C in 5% CO_2 in air and 95%–97% relative humidity. At 44 h of maturation, a representative group of COC was snap-frozen and storage at −80°C until further analyses.

In vitro fertilization (IVF)

Following IVM, matured COC were denuded through vortexing at 200 × *g* for 2 min in 400 µL of TL-HEPES-PVA containing 0.1 mg/mL hyaluronidase. Subsequently, denuded oocytes were washed three times in both IVM and IVF medium. The IVF medium, comprising Tris-buffered medium supplemented with 2 mM caffeine and 0.2 mg/mL bovine serum albumin (BSA). Groups of 35 – 40 oocytes were then positioned in 50-µL drops of IVF medium and co-incubated with frozen-thawed spermatozoa, prepared according to the method outlined by Gil et al (2017). For each replicate, a semen straw was thawed at 37 °C for 20 s, and 200 µL of sperm underwent three washes in Dulbecco's phosphate-buffered solution (dPBS) containing 4% BSA via centrifugation at 1,900 × *g* for 3 min. The resulting pellet was resuspended in IVF medium, and 50 µL of extended spermatozoa were added to the 50 µL drop containing the oocytes. This mixture was co-incubated under paraffin oil at 38.5 °C with 5% CO_2 and saturated humidity for 5 h. The sperm: oocyte proportion used was 1,000:1.

In vitro culture (IVC)

Following IVF, the presumptive zygotes underwent a washing procedure by repeated pipetting in IVC medium to eliminate any spermatozoa attached to the zona pellucida (ZP). The culture medium for the subsequent embryo development was based on the formulation from North Carolina State University 23 (NCSU-23) enriched with 0.3 mg/mL PVA and 0.4% BSA. Subsequently, groups of 40 presumptive zygotes were incubated in 500 µL of IVC medium containing pyruvate (0.3 mM) and lactate (4.5 mM) during the initial 2 d of the culture period. Further culture was conducted in 500 µL of fresh IVC medium containing glucose (5.5 mM) for additional 5 d. Throughout the IVC period, the conditions were consistently maintained under paraffin oil at 38.5 °C, in a 5% CO_2 in air, and with saturated humidity.

Evaluation of IVM, IVF, and embryo development rates

Denuded oocytes and presumptive zygotes were fixed 44 h after IVM and 18 h after IVF, respectively in a PBS solution with 0.5% (v/v) glutaraldehyde for 30 min. The fixed samples were placed in 2-µL drops of Vectashield (Vector, Burlingame, CA, USA) containing 10 mg/mL Hoechst 33342 on a slide and covered with a coverslip. The samples were observed under a fluorescence microscope (excitation filter 330 to 380 nm) at 400× magnification. The oocytes were considered immature when the chromatin was enclosed in a nuclear membrane or condensed in metaphase I, whereas they were classified as mature when the chromatin was organized in metaphase and the first polar body was visible (metaphase II). Maturation rate was defined as the number of oocytes in metaphase II relative to the total number of oocytes stained. The oocytes were considered penetrated when at least two pronuclei were visible in the cytoplasm. In addition,

when there were only two pronuclei, the monospermic status was confirmed. The subset of penetrated oocytes relative to the mature oocytes was defined as penetration rate. Monospermic rate was calculated as the number of monospermic oocytes relative to the number of penetrated oocytes. Efficiency of fertilization was calculated as the percentage of monospermic oocytes over the total number of presumptive zygotes.

To assess the progression of embryo development, we examined cleavage, blastocyst formation rates, and overall IVP efficiency. Cleavage rate was determined as the percentage of embryos reaching the 2- to 4-cell stage on d 2 relative to the total number of inseminated oocytes. Blastocyst yield on d 6 and 7 was calculated as the ratio of embryos at the blastocyst stage to the total number of cleaved embryos. Ultimately, total IVP efficiency was quantified as the percentage of embryos reaching the blastocyst stage by d 7 relative to the total number of inseminated oocytes.

RNA extraction

Total RNA was isolated from oocytes and embryos using a miRNeasy Micro Kit (Qiagen Iberica, Madrid, Spain), following manufacturer's instructions. The quantity and quality of the RNA obtained were analyzed using a Nanodrop 2000 (ThermoFisher Scientific, Madrid, Spain) and a Bioanalyzer 2100 (Agilent, Santa Clara, CA, USA). RIN values were higher than eight for all samples.

RNA-seq

RNA-seq libraries were prepared using the Stranded Total RNA Prep Ligation with Ribo-Zero Plus kit (Illumina, USA, Cat. # 20040525), which enables depletion of ribosomal RNA and preserves strand information. Library preparation was carried out according to the manufacturer's protocol, starting from low-input total RNA. Briefly, ribosomal RNA was first depleted using the Ribo-Zero Plus chemistry. The remaining RNA was then fragmented and converted into double-stranded cDNA. After end repair and adaptor ligation, libraries were PCR-amplified and purified to remove adaptor dimers and short fragments. Library size distribution and quality were evaluated using the Bioanalyzer prior to sequencing. Sequencing was performed with the NextSeq 500/550 High Output Kit v2.5 (150 cycles), employing a 2×75 base pair paired-end read configuration. Raw sequencing data have been deposited in the NCBI Sequence Read Archive (SRA) under accession number SUB15922627.

Statistical analysis

Raw sequencing data were processed and analyzed using Partek Flow software. Reads were quality-checked, trimmed when necessary, and aligned to the *Sus scrofa* reference genome using the STAR aligner (Dobin et al 2013). Alignment was performed using default parameters, allowing for spliced alignments, with a maximum of 10 multiple alignments per read and up to 10 mismatches per read (mismatch ratio ≤ 0.3). A minimum intron length of 21 bp was required. Local alignment mode was applied, and two-pass mapping was not used. An average of 22.7 million paired-end reads per sample was obtained, with sequencing depth ranging from approximately 50 to 68 million reads across samples. Gene-level counts were normalized using the DESeq2 median-of-ratios method, which corrects for library size and compositional bias across samples.

Differential gene expression between developmental stages was assessed using DESeq2, and genes with a false discovery rate (FDR) <0.05 were considered as significantly differentially expressed. For selected analyses, an additional fold-change cutoff of >2 was applied as indicated. DEGs were identified and further analyzed for functional classification and stage-specific expression patterns. To gain insights into the functional implications of these DEGs, enrichment analyses were conducted using the DAVID bioinformatics toolset, incorporating annotations from the KEGG (Kyoto Encyclopedia of Genes and Genomes) and DICE (Database of Immune Cell Expression) databases. The background gene list consisted of all genes detected in the RNA-seq dataset after filtering, which served as the reference population in DAVID. Functional annotation clustering and gene ontology categorization were used to identify significantly overrepresented biological processes.

Results

Oocyte and embryo development rates

Oocyte maturation, fertilization efficiency, and embryo development rates were evaluated at 44 h of IVM, 18 h post-IVF, and d 2, 6, and 7 of IVC, respectively (Figure S1, see online supplementary material for a color version of this figure). We had an overall oocyte maturation rate of $90.42 \pm 1.78\%$. After IVF, penetration, monospermy, and fertilization efficiency were $66.66 \pm 0.08\%$, $54.71 \pm 0.11\%$, and $30.53 \pm 0.04\%$, respectively. Embryo development progressed with a cleavage rate of $67.55 \pm 0.05\%$, blastocyst formation rate of $56.81 \pm 0.02\%$ and final efficiency rate of $37.87 \pm 0.03\%$. Finally, $12.34 \pm 0.02\%$ of blastocysts were hatching or hatched on d 7 of IVC.

Global transcriptional dynamics reveal major stage transitions during early porcine oocyte-embryo development

To obtain a global overview, we compared gene expression profiles among groups. Principal component analysis (PCA) showed clear clustering by developmental stage, where IMO and MO grouped together but remained clearly separated along PC1, zygotes and cleaved embryos clustered in proximity, and blastocysts occupied a distant region of multivariate space (Figure 1A). Differential gene expression analysis revealed significant changes between groups. We identified 1,835 DEGs (816 upregulated, 1,019 downregulated) in MO vs IMO, 6,590 DEGs (3,247 upregulated, 3,343 down-upregulated), in ZY vs MO, only 201 DEGs (115 upregulated, 86 downregulated) in CL vs ZY, and 6,301 DEGs (3,130 upregulated, 3,171 downregulated) in BL vs CL. Volcano plots for each comparison (Figure 1B–E) illustrate the magnitude of transcriptional changes, while a Venn diagram (Figure 1F) revealed the extent of gene overlap between transitions, identifying sets of DEGs unique to specific developmental windows and others shared across multiple comparisons.

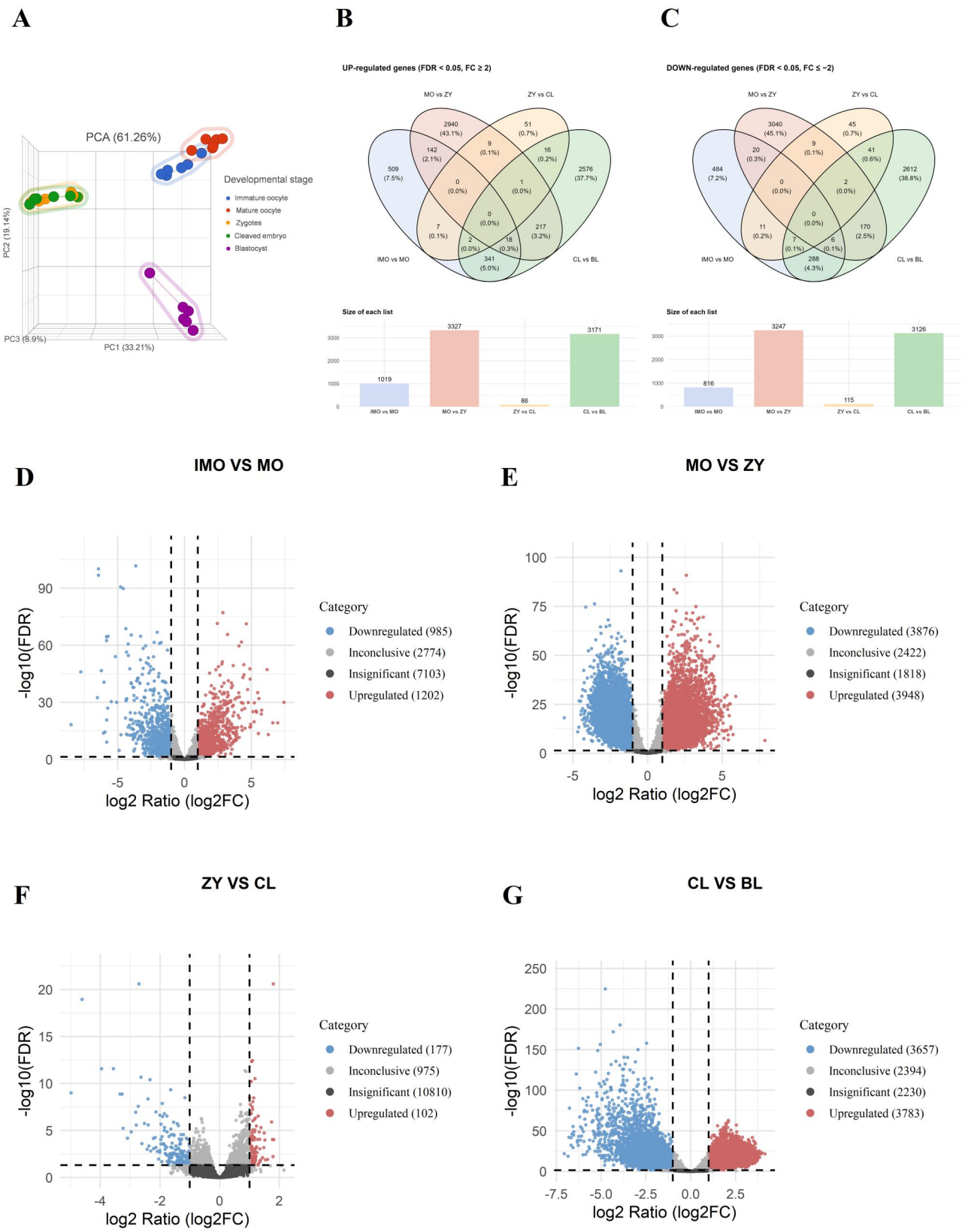

Figure 1 Differential gene expression profiling across consecutive developmental transitions during oocyte maturation and early embryogenesis. A) Principal component analysis. Panels B) and C) depict Venn diagrams showing commonly dysregulated genes among comparisons. D) to G) Volcano plots illustrating differential gene expression between comparisons.

Distinct expression modules of canonical and non-canonical WNT components across early developmental stages

To characterize how the WNT signaling pathway is organized across early porcine embryo development, we examined the expression patterns of all WNT-related genes using heatmap clustering and network analyses. Figure 2 summarizes the stage-specific modulation of WNT signaling components across porcine early oocyte-embryo development. Bar plots representing WNT functional modules revealed marked differences in the number and direction of differentially expressed genes (FDR < 0.05) between consecutive developmental stages (Figure 2A). The largest reorganization of WNT-related transcripts occurred during the transitions from IMO to MO and from CL to BL, whereas ZY and CL embryos showed highly similar expression profiles, with comparatively few differentially expressed WNT genes. Heatmap visualization of WNT-associated genes across all stages further highlighted these patterns, clustering IMO and MO separately from post-fertilization stages, while ZY and CL embryos appeared grouped closely together (Figure 2B). In addition, network representations of WNT genes illustrated dynamic changes in pathway architecture, with distinct connectivity patterns emerging during oocyte maturation and blastocyst formation (Figure 2C).

Stage-specific regulation of WNT-related specific components across oocyte maturation and early embryonic development

The expression of individual WNT pathway genes displayed clear, stage-dependent changes across the oocyte-to-embryo transition (Tables 1–3; Figure 3). The antagonists *DKK1*, *DKK3*, and *FRZB* were significantly upregulated in MO vs IMO, and subsequently downregulated in ZY and CL groups. These genes remained low or unchanged at the BL stage. Frizzled receptors showed divergent expression patterns. *FZD3* and *FZD4* were upregulated in MO vs IMO, while *FZD6* and *FZD7* were downregulated in the same comparison. After fertilization, several receptors (*FZD3*, *FZD4*, *FZD5*, *FZD8*) were reduced in ZY vs MO, with similar expression profiles in CL embryos. Co-receptors displayed comparable dynamics: *LGR4*, *ROR1*, and *RYK* decreased progressively from IMO to BL. Among ligand-encoding genes, *WNT2B*, *WNT3*, and *WNT7A* were downregulated in MO vs IMO, but upregulated in ZY and CL embryos, followed by a reduction in BL. Elements of the β-catenin destruction complex—including *AXIN2*, *APC*, and *GSK3B*—were upregulated in MO vs IMO. After fertilization, these genes showed reduced or stable expression across ZY and CL stages, with further changes detected at the BL stage. *LEF1* was low in MO, increased in ZY and CL embryos, and was reduced again in BL. PCP-associated and adhesion-related genes exhibited distinct stage-dependent profiles. *CTNND2* showed markedly higher expression in MO compared with all other stages, where it remained low. Conversely, *CTNND1* was upregulated in ZY, CL, and BL vs MO. PCP regulators such as *PRICKLE2* and *DAAM1* increased progressively toward the BL stage.

Discussion

In the present study, we investigated the regulatory dynamics of WNT signaling components during porcine oocyte and early embryo development. Using the selected thresholds (FDR <0.05; |Fold Change| ≥ 2), we identified 112 WNT-related genes differentially expressed among groups. Notably, *DKK1* and *DKK3* (Dickkopf Wnt Signaling Pathway Inhibitor 1 and 3) genes, were significantly upregulated in MO compared with IMO. DKK1 and DKK3 are high-affinity extracellular antagonist that bind the WNT co-receptors LRP5/6 (low density lipoprotein receptor protein 5 and 6) (Semënov et al 2001). These co-receptors work alongside Frizzled (FRZ) receptors to regulate key cellular processes like development and homeostasis in the canonical WNT/β-catenin signaling pathway (Ren et al 2021). By blocking the formation of the FZD–LRP signalosome, DKK1 and DKK3 prevent β-catenin stabilization and thus they maintain the canonical pathway in an inactive state. In agreement with this inhibitory mechanism, *LRP5* gene expression was indeed downregulated in MO vs IMO groups, suggesting that DKK1/3-mediated suppression occurs at this stage. Overall, these findings support a model of late-stage "gating" of canonical WNT signaling, in which β-catenin activity is restrained as meiosis completes to prevent premature transcriptional activation before fertilization. Consistently, studies in pig and buffalo COC have shown that supplementation with DKK proteins during IVM enhances oocyte maturation and improves subsequent embryo quality (Spate et al 2014; Ahuja et al 2023). Interestingly, the expression of FZD receptors showed a divergent pattern between IMO and MO groups, with *FZD3* and *FZD4* genes upregulated and *FZD6* and *FZD7* downregulated in MO compared with IMO. This likely reflects functional specialization among FZD family members, which can preferentially engage different WNT ligands and downstream branches of the pathway. FZD3 and FZD4 proteins are typically associated with non-canonical (planar cell polarity and Ca^{2+}-dependent) signaling, which contributes to cytoskeletal remodeling, spindle anchoring, and cortical polarity-key events at the end of meiosis (Pourreyron et al 2012). In contrast, FZD6 and FZD7 are more frequently linked to canonical β-catenin signaling and to transcriptional regulation during cell proliferation and fate determination (Liu et al 2024). Their downregulation at Metaphase II therefore aligns with the suppression of canonical WNT activity observed through the upregulation of DKK1/3.

In addition, Secreted FRZ-Related Protein 3 (SFRP3) is a soluble protein that resembles a FRZ receptor and can bind WNT ligands in the extracellular space (Zi et al 2005). By capturing these ligands, SFRP3 acts as a "WNT trap," reducing the amount of free WNT that can reach its receptors and therefore weakening WNT signaling (Oldefest et al 2015). SFRP3 is produced mainly by ovarian somatic cells, including cumulus and granulosa cells, where it helps regulate the microenvironment surrounding the oocyte. Experimental studies (for example, those showing that SFRP3 can disrupt the WNT10B–FZD7 interaction in trophoblast and epithelial cells [Larasati et al 2022]) support its antagonistic role as a ligand buffer in the extracellular space. In our dataset, *SFRP3* was up regulated in MO compared with IMO. This is consistent with a cumulus-derived system that reduces free WNT ligands around the mature oocyte, limiting canonical β-catenin–dependent transcription and instead favoring

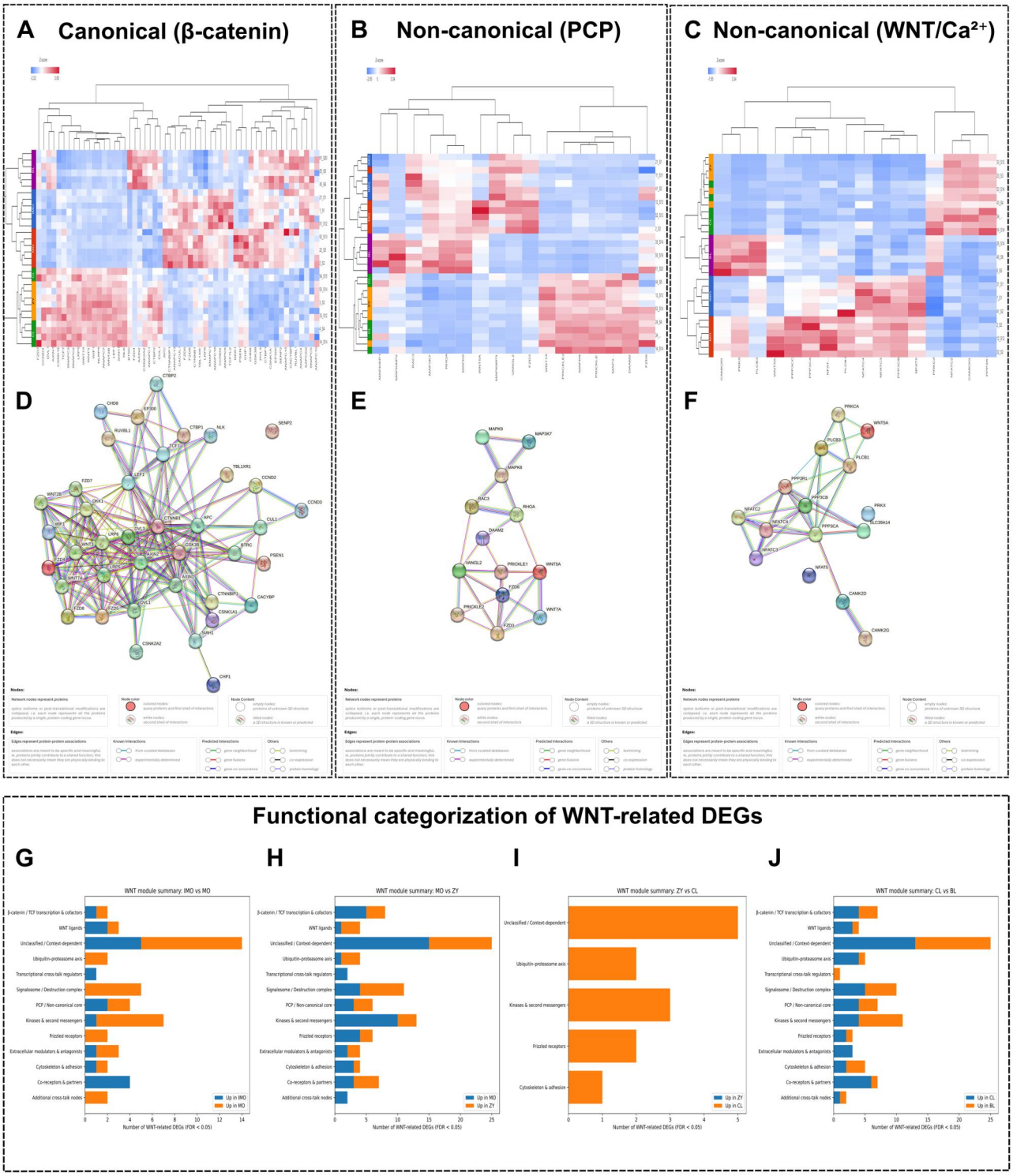

Figure 2 Supervised hierarchical clustering and network analyses of differentially expressed genes (FDR < 0.05 and $|FC| \geq 2$) associated with WNT signaling pathway. Panels A) and D) show the supervised hierarchical clustering and the corresponding STRING-based protein–protein interaction (PPI) network of genes related to the canonical WNT signaling pathway. Panels B) and E) display the supervised hierarchical clustering and the representative PPI network of genes associated with the non-canonical planar cell polarity (PCP) WNT signaling pathway. Panels C) and F) illustrate the supervised hierarchical clustering and the representative PPI network of genes related to the non-canonical calcium-dependent WNT signaling pathway. PPI networks were generated using STRING (v11.5) for *Sus scrofa*, considering the full STRING network and a minimum interaction score of 0.400 (medium confidence), and including only query proteins (no additional interactors). Panels G) to J) present bar charts summarizing the number of up- and downregulated transcripts within major WNT signaling modules among comparisons: G) IMO vs. MO, H) MO vs. ZY, I) ZY vs. CL, and J) CL vs. BL.

Table 1 Differentially expressed transcripts related to the WNT canonical pathway among comparisons.

Gene	Category	FDR step up MO vs. IMO	Fold change MO vs. IMO	FDR step up ZY vs. MO	Fold change ZY vs. MO	FDR step up CL vs. ZY	Fold change CL vs. ZY	FDR step up BL vs. CL	Fold change BL vs. CL
DVL1	Dvl (dishev-			<0.001	3.645				
DVL2	elled) proteins								
DVL3				<0.001	−2.996			<0.001	2.275
CTNNBIP1	Inhibitors			<0.001	−2.864				
CXXC4									
DKK1		<0.001	57.348	<0.001	−7.047			<0.001	−4.983
DKK3		<0.001	3.848	<0.001	−15.72				
FRZB		<0.001	−7.919	<0.001	7.698			<0.001	−6.082
NLK				<0.001	2.753			<0.001	−3.611
WIF1				<0.001	7.199			<0.001	−8.543
APC	Intracellular			<0.001	−3.011			<0.001	−1.771
AXIN1	components			<0.001	1.984			0.033	−1.365
AXIN2		<0.001	2.109	0.040	1.326			<0.001	2.053
BTRC				<0.001	1.521			0.001	1.447
CACYBP				<0.001	−1.702			<0.001	3.200
CCNY				<0.001	1.952	0.014	1.244	<0.001	−2.070
CHD8				<0.001	−3.758			<0.001	2.353
CSNK1A1				<0.001	−2.051			<0.001	2.088
CSNK1D				<0.001	1.303			0.005	−1.310
CSNK1E				<0.001	1.747			<0.001	−3.114
CSNK2A2				<0.001	1.363				
CSNK2B						0.016	1.330		
CTNNB1				0.021	−1.235			0.018	−1.246
CTNND1				<0.001	2.790			<0.001	−1.602
CUL1				<0.001	2.108				
FBXW11						0.038	1.244	<0.001	−2.009
FRAT2						<0.001	9.648		
GSK3A				<0.001	1.850			<0.001	−1.321
GSK3B				<0.001	−5.650			<0.001	2.371
LZIC				<0.001	4.150	0.046	1.270	<0.001	−3.802
NHERF1								<0.001	19.673
PSEN1		<0.001	2.194	<0.001	−1.558			<0.001	−1.396
SENP2				<0.001	−1.693			<0.001	1.722
SIAH1				<0.001	4.631			<0.001	−3.726
SIAH2		<0.001	4.797	<0.001	−8.755			0.001	1.536
SKP1						0.001	1.292	<0.001	−1.578
WNT2B	Ligands			<0.001	5.528			<0.001	−4.087
WNT3				<0.001	9.734			<0.001	−4.107
CREBBP	Nuclear							0.038	−1.150
CTBP1	effectors			<0.001	−2.004			<0.001	1.829
CTBP2				<0.001	2.742				
CTNNB1				0.021	−1.235			0.018	−1.246
EP300				<0.001	−2.407			<0.001	2.550
HDAC1				<0.001	−4.794			<0.001	3.676
LEF1				<0.001	9.206			<0.001	−11.056
RUVBL1				<0.001	−2.149			<0.001	3.247
SMAD3				<0.001	−2.859				
SMAD4		0.038	−2.150	<0.001	−5.593			0.014	2.228
TBL1XR1				<0.001	−1.936			<0.001	−2.322
TCF7				0.037	1.506			<0.001	−5.559
TCF7L2		<0.001	−4.490					0.050	−1.363
TLE3				<0.001	−4.984			<0.001	5.907

(continued)

Table 1 (continued)

Gene	Category	FDR step up MO vs. IMO	Fold change MO vs. IMO	FDR step up ZY vs. MO	Fold change ZY vs. MO	FDR step up CL vs. ZY	Fold change CL vs. ZY	FDR step up BL vs. CL	Fold change BL vs. CL
TLE4				0.025	1.229	0.048	1.285		
FGFR2	Receptors/ coreceptors	<0.001	7.514	<0.001	−5.287			<0.001	4.198
FZD4				<0.001	−2.204	0.005	1.960	<0.001	11.018
FZD5				<0.001	−3.342				
FZD7				0.015	1.698	<0.001	3.616	<0.001	−2.372
FZD8				<0.001	−4.372				
GPC4				<0.001	−3.393			<0.001	−4.015
KREMEN1				<0.001	3.426			0.013	−1.265
LGR4		<0.001	−4.527					<0.001	−2.097
LRP4				<0.001	9.057			<0.001	−11.178
LRP5				<0.001	4.181			<0.001	−5.943
LRP6				0.001	−1.366			<0.001	−2.711
ZNRF3				<0.001	1.724			<0.001	−1.717
CCND2	Transcriptional target genes			<0.001	−6.917				
CCND3				<0.001	2.056			0.001	−1.558
PPARD								<0.001	−2.531

For key biological transcripts a less restrictive Fold Change cut off was used.
Fold change with positive or negative values indicating higher or lower expression, respectively, in the first group listed.

Table 2 Differentially expressed transcripts related to the WNT non-canonical (PCP) pathway among comparisons.

Gene	Category	FDR step up MO vs. IMO	Fold change MO vs. IMO	FDR step up ZY vs. MO	Fold change ZY vs. MO	FDR step up CL vs. ZY	Fold change CL vs. ZY	FDR step up BL vs. CL	Fold change BL vs. CL
CCDC88C	Intracellular components			<0.001	3.421			<0.001	−5.153
DAAM1								<0.001	−3.310
DAAM2				<0.001	9.671			<0.001	−5.707
INVS				<0.001	−2.940				
PRICKLE1				<0.001	5.995			<0.001	−11.069
PRICKLE2		<0.001	−2.288	<0.001	6.777			<0.001	−8.293
PRICKLE3				<0.001	−6.701			<0.001	16.185
RAC1						0	1.531	<0.001	1.620
RAC3		<0.001	−2.285	0.001	−2.222			0.001	2.221
RHOA				<0.001	−2.947			<0.001	4.807
ROCK2								<0.001	1.646
VANGL1								<0.001	1.570
VANGL2				<0.001	−13.067				
WNT5A	Ligands	<0.001	5.386	<0.001	−4.445			0.005	1.795
WNT7A				<0.001	10.750			<0.001	−5.941
FOSL1	Nuclear effectors			0.011	−2.532				
JUN		<0.001	−9.474						
CELSR1	Receptors/ coreceptors	<0.001	2.499	<0.001	−1.858			<0.001	11.663
FZD3				<0.001	−2.643			<0.001	−1.951
FZD6				0.001	1.658				
ROR1		0.001	−2.237	<0.001	−3.635			<0.001	3.860
RYK		0.008	−2.083	<0.001	−4.642				
MAP3K7	Transcriptional target genes			<0.001	−2.276			<0.001	2.322
MAPK8				<0.001	2.622			<0.001	−5.679
MAPK9				<0.001	−4.119			<0.001	4.795

For key biological transcripts a less restrictive Fold Change cut off was used.
Fold change with positive or negative values indicating higher or lower expression, respectively, in the first group listed.

Table 3 Differentially expressed transcripts related to the WNT non-canonical (Ca^{+2}) pathway among comparisons.

Gene	Category	FDR step up MO vs. IMO	Fold change MO vs. IMO	FDR step up ZY vs. MO	Fold change ZY vs. MO	FDR step up CL vs. ZY	Fold change CL vs. ZY	FDR step up BL vs. CL	Fold change BL vs. CL
CAMK2D	Intracellular components	<0.001	2.642	<0.001	−3.045			<0.001	6.546
CAMK2G				<0.001	2.264			<0.001	−3.309
PLCB1				<0.001	−2.945				
PLCB3				<0.001	−3.693			<0.001	12.578
PPP3CA		0.013	2.271	<0.001	−15.20			0.017	2.078
PPP3CB				<0.001	−4.034			0.041	−1.316
PPP3CC		<0.001	2.286	<0.001	−3.755			<0.001	1.750
PPP3R1				<0.001	1.929	0.013	1.349	<0.001	−2.516
PRKACA				<0.001	−3.883	<0.001	1.506	<0.001	1.520
PRKACB				<0.001	−2.156			<0.001	−4.674
PRKCA		<0.001	2.053	0.015	1.396	0.042	1.463		
NFATC1	Nuclear effectors	<0.001	−5.333					0.001	3.247
NFATC2		<0.001	−2.932	<0.001	8.216			<0.001	−4.250
NFATC2IP		<0.001	2.510	<0.001	−6.136			0.035	1.463
NFATC3				<0.001	−3.363			0.019	1.252
NFATC4				<0.001	−2.299			0.009	−2.191

For key biological transcripts a less restrictive Fold Change cut off was used.
Fold change with positive or negative values indicating higher or lower expression, respectively, in the first group listed.

non-canonical, mechanically oriented signaling (Canonical WNT off/non-canonical WNT on). Taken together, these opposite trends suggest a shift in WNT receptor usage; as maturation proceeds, the oocyte reduces receptors driving β-catenin–dependent transcription (FZD6/7) while maintaining or increasing those that favor non-canonical, mechanically oriented signaling (FZD3/4). This selective tuning likely supports the cytoskeletal and structural reorganization necessary for oocyte competence while preventing unwanted transcriptional activation before fertilization.

On the other hand, WNT family member 5A (*WNT5A*) gene expression was also found up-regulated in MO vs IMO. WNT5A is a secreted ligand that biases non-canonical WNT outputs (PCP/Ca^{2+}) and can antagonize canonical β-catenin in certain contexts; in COCs it engages Mitogen-activated protein kinases (MAPK) activity and cytoskeletal programs (Rogers and Scholpp 2022). In pigs, supplementation with WNT5A (together with CXCL12/VEGFA) promotes oocyte maturation, enhances cumulus expansion, increases blastocyst cell number, and is linked to MAPK activation with canonical WNT inhibition (Liu et al 2020). Our results are in line with a switch toward non-canonical/PCP–Ca^{2+} signaling at the end of maturation that supports cortical remodeling and mechanical readiness for fertilization while keeping β-catenin transcription gated.

Leucine-Rich Repeat–Containing G Protein-Coupled Receptor 4 *(LGR4*) is a membrane receptor that binds R-spondins (RSPO1/2/3) (Peng et al 2025). This interaction enhances WNT signaling by blocking the activity of two proteins (ZNRF3 and RNF43) that normally reduce the number of WNT receptors (frizzled) at the cell surface. In this way, LGR4 helps to increase WNT sensitivity in epithelial and reproductive tissues. In our study, *LGR4* expression was lower in MO than in IMO. When considered together with the higher levels of WNT antagonists (*DKK1, DKK3, SFRP3*) in MO, this suggests that IMO are pre-set for strong WNT responsiveness, whereas during maturation, this sensitivity is reduced or balanced to prevent premature β-catenin activation before fertilization. Taken together, these opposite trends suggest a shift in WNT receptor usage: as maturation proceeds, the oocyte reduces receptors driving β-catenin-dependent transcription (FZD6/7) while maintaining or increasing those that favor non-canonical, mechanically oriented signaling (FZD3/4).

Catenin Beta 1 (*CTNNB1*), also known as β-catenin, is the main effector of the canonical WNT pathway and plays two key roles—it supports cell adhesion and also regulates gene transcription (Van Der Wal and Van Amerongen 2020). When WNT signaling is inactive, β-catenin is continuously marked for degradation by a group of proteins called the destruction complex, which includes AXIN1/2, Adenomatous Polyposis Coli (APC), Casein Kinase 1 (CK1), and Glycogen Synthase Kinase 3 (GSK3) (Stamos and Weis 2013). When WNT becomes active, this complex is inhibited, allowing β-catenin to accumulate in the cytoplasm and move into the nucleus, where it binds to T-Cell Factor (TCF) and Lymphoid Enhancer-Binding Factor (LEF) to turn on WNT-responsive genes (Ranes et al 2021). The increased expression of *AXIN2*, *APC*, and *GSK3B* in MO compared to IMO supports the idea that it acts as part of a feedback system that re-establishes β-catenin degradation, ensuring that canonical signaling is switched off by the end of maturation. This pattern indicates that canonical WNT signaling may occur only briefly during maturation and is then actively suppressed to maintain the transcriptional silence required at the MII stage. This regulation ensures that canonical WNT signaling remains available for use after fertilization while maintaining the transcriptional silence essential for meiotic completion and developmental competence yet preserves non-canonical/PCP and Ca^{2+} arms that assist cytoskeletal/cortical remodeling.

Once fertilization occurs and the zygote initiates zygotic genome activation, this inhibitory control in the extracellular

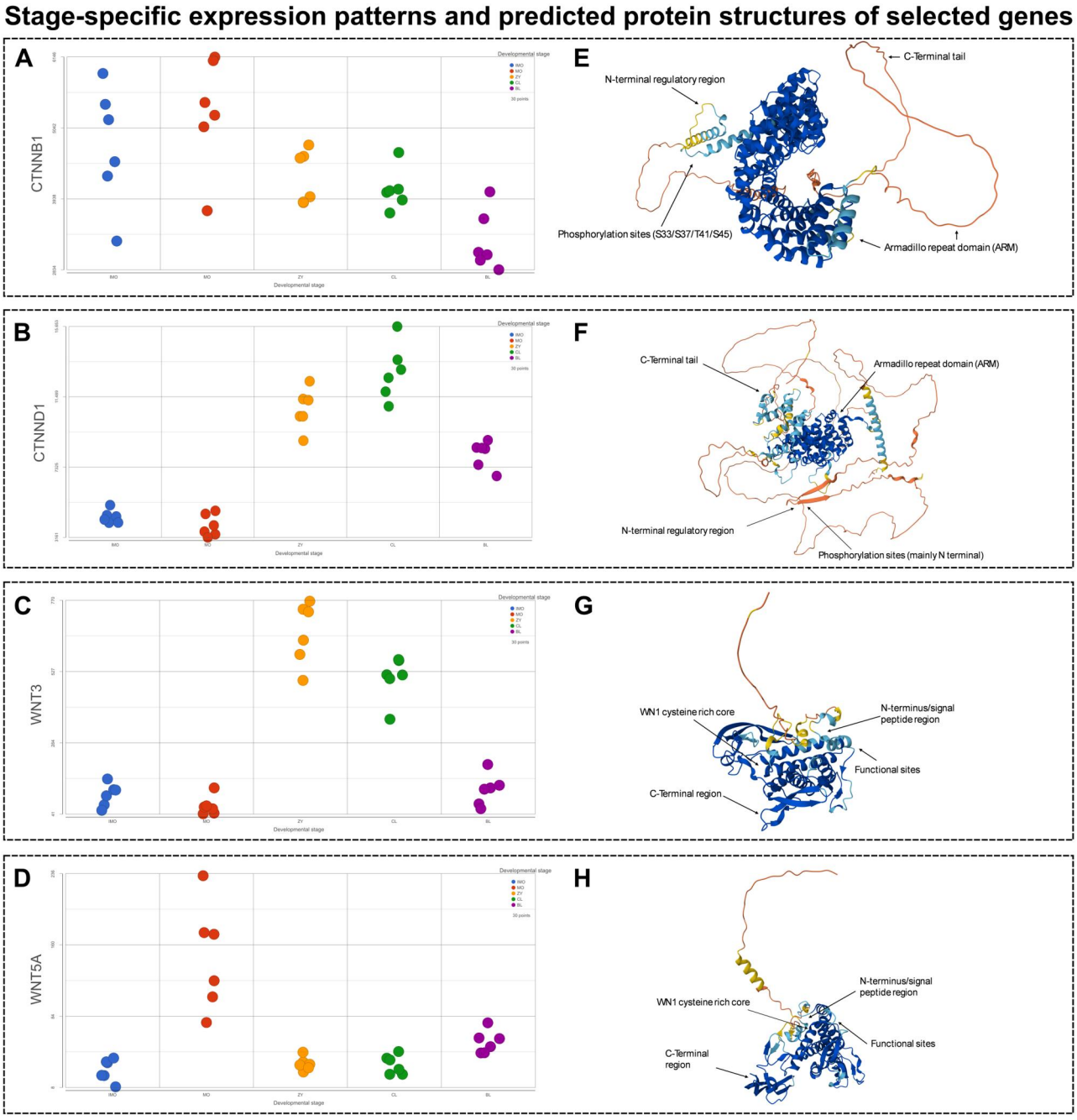

Figure 3 Stage-specific expression patterns and predicted protein structures of selected genes in porcine oocyte and early embryo development (*CTNNB1, CTNND1, WNT3, WNT5A*). A) to D) Scatter plots showing normalized gene expression levels (log_2 scale) of selected WNT pathway–related genes across different stages of porcine oocyte and early embryo development. E) to H) Predicted protein structures of WNT ligands, emphasizing the characteristic cysteine-rich core, the N-terminal signal peptide region associated with secretion and signaling, key functional sites, and the C-terminal region.

space is no longer required. The subsequent decline in *DKK1* and *DKK3* expression in ZY vs MO enables a re-sensitization to WNT signals, allowing the embryo to re-engage both canonical and non-canonical WNT pathways essential for early cell polarity, cleavage, and lineage specification.

In contrast, we observed a selective reduction of Frizzled receptors—notably *FZD3, FZD4, FZD5*, and *FZD8* decreased in ZY compared with MO—together with modest, stage-close changes between ZY and CL (eg *FZD7* decreased). This pattern indicates a transient dampening of surface WNT reception at the very onset of development, consistent with the need to avoid premature or excessive β-catenin signaling while the embryo transitions from maternal control toward zygotic control. In other words, the zygote reopens the window for WNT signaling but keeps it under strict regulation to ensure a controlled transition toward embryonic genome activation.

On the other hand, the upregulation of *CTNND1* (Catenin Delta-1) gene in ZY, CL, and BL compared with MO suggests the activation of adhesion and polarity mechanisms immediately after fertilization. CTNND1 plays a central role in maintaining cell–cell adhesion and epithelial organization, two processes that are progressively established as the embryo transitions from a single cell to a multicellular structure (Davis et al 2003). Its continued expression suggests that cadherin-based junctions and cytoskeletal anchoring become increasingly important for blastomere cohesion, compaction, and blastocoel cavity formation. Beyond adhesion, CTNND1 also acts as a modulator of WNT signaling by regulating β-catenin availability and Rho-family GTPase activity (Hernández-Martínez et al 2019). During cleavage and blastocyst formation, this dual function may help coordinate cell polarity and signaling gradients, ensuring proper lineage segregation between the inner cell mass and trophectoderm.

Furthermore, *LEF1* (Lymphoid Enhancer-Binding Factor 1), a nuclear transcription factor that partners with β-catenin to drive canonical WNT-dependent gene expression was found low in MO vs IMO, increased in ZY and CL vs MO, then reduced again in BL vs CL. During the MII stage, the oocyte is transcriptionally quiescent, and after fertilization, as the embryo enters the maternal-to-zygotic transition, increased *LEF1* suggests that the embryo is reacquiring canonical WNT transcriptional competence, enabling early cell-cycle progression, cleavage-stage polarity cues, and the first lineage-priming events. This transient rise is consistent with reports that LEF/TCF factors are among the early transcriptional responders during zygotic genome activation in mammals (Ross et al 2025). However, once the embryo reaches the blastocyst stage, developmental priorities shift from transcriptional activation to epithelial organization, lumen formation, and lineage segregation. These processes rely more heavily on non-canonical WNT/PCP signaling, adhesion molecules, and Hippo–TEAD pathways, reducing the need for strong β-catenin-LEF1 transcription.

We observed an interesting dynamic for WNT ligand expression in our dataset. *WNT2B, WNT3*, and *WNT7A* (genes encoding ligands primarily associated with canonical WNT/β-catenin signaling) were downregulated in MO vs IMO, increased in ZY and CL, then reduced again in BL. Their post-fertilization upregulation likely reflects the onset of zygotic genome activation, when the embryo briefly needs canonical WNT inputs to support cell-cycle progression, cleavage timing, chromatin remodeling, and early lineage priming. This transient rise suggests that the embryo becomes temporarily competent to receive and integrate WNT cues, consistent with the re-expression of downstream transcriptional mediators such as LEF1. Their repression toward the blastocyst state is consistent with a shift toward non-canonical WNT/PCP signaling.

Together, these transcriptomic data reveal that porcine oocytes and early embryos undergo a coordinated, stage-specific restructuring of WNT signaling. Maturation establishes a WNT-competent but transcriptionally restrained state, dominated by extracellular antagonism and non-canonical signaling, apparently supporting cytoskeletal remodeling and meiotic completion. Fertilization then seems to trigger a transient reactivation of selected WNT ligands, transcriptional mediators, and adhesion regulators, aligned with zygotic genome activation and early cleavage organization. By the blastocyst stage, WNT activity appears to become spatially refined and increasingly linked to polarity and epithelial architecture. This dynamic progression suggests that precise temporal control—not global activation—of WNT signaling is fundamental for successful pig preimplantation development.

Limitations of the study: All oocytes and embryos analyzed in this study were produced under in vitro conditions (IVM/IVF/IVC), which are known to influence gene expression profiles compared to *in vivo*-derived counterparts. However, the controlled in vitro system used here provides a consistent framework to investigate relative, stage-specific transcriptional dynamics. A further limitation of this study is that individual pronuclear confirmation was not performed prior to pooling zygote samples for RNA-seq, due to the technical difficulty of visualizing pronuclei in lipid-rich porcine zygotes. Therefore, the inclusion of a proportion of unfertilized oocytes in the zygote group cannot be fully excluded, although the marked transcriptional divergence from mature oocytes and the clustering of zygotes with cleavage-stage embryos support their classification as post-fertilization samples. Furthermore, porcine IVF is inherently associated with a relatively high incidence of polyspermy, particularly when using frozen-thawed semen. Therefore, the presence of polyspermic zygotes cannot be ruled out and should be considered when interpreting early post-fertilization transcriptomic profiles.

Acknowledgments

We are grateful to the staff of the local slaughterhouse (Comarán S.L., Madrid, Spain) for their assistance and for providing offal ovaries for this study. We also acknowledge the Core Facility at the Faculty of Medicine and Health Sciences, Linköping University for providing assistance for RNA-Sequencing service.

Funding

This work was supported by MICIU/AEI/10.13039/501100011033 and ERDF/EU (Project PID2023-150622OA-100), and by the LiU-Agropor research agreement (86037-293205).

Author contributions

Carolina G. Cabrera-Gomez (Methodology, Writing—original & draft), David Gascon-Collado (Methodology, Writing—review & editing), Paula Blanco-Cueto (Methodology, Writing—review & editing), Belen Pequeño (Methodology, Writing—review & editing), and Heriberto Rodriguez-Martinez (Conceptualization, Funding acquisition, Project administration, Writing—review & editing)

Supplementary data

Supplementary data are available at *Journal of Animal Science* online.

Conflict of interest statement. The authors declare no real or perceived conflicts of interest.

References

Ahuja K, Batra V, Kumar R, Datta TK. 2023. Transient suppression of Wnt signaling in poor-quality buffalo oocytes improves their developmental competence. Front Vet Sci. 10:1324647. https://doi.org/10.3389/FVETS.2023.1324647/BIBTEX

Bazer FW, Johnson GA. 2014. Pig blastocyst-uterine interactions. Differentiation. 87:52–65. https://doi.org/10.1016/j.diff.2013.11.005

Davis MA, Ireton RC, Reynolds AB. 2003. A core function for p120-catenin in cadherin turnover. J Cell Biol. 163:525–534. https://doi.org/10.1083/JCB.200307111

Dobin A et al. 2013. STAR: ultrafast universal RNA-seq aligner. Bioinformatics. 29:15–21. https://doi.org/10.1093/BIOINFORMATICS/BTS635.

Domínguez-Oliva A et al. 2023. The importance of animal models in biomedical research: current insights and applications. Animals (Basel). 13:1223. https://doi.org/10.3390/ANI13071223

Fuentes R et al. 2024. Maternal regulation of the vertebrate oocyte-to-embryo transition. PLoS Genet. 20:e1011343. https://doi.org/10.1371/JOURNAL.PGEN.1011343

Gil MA et al. 2017. Effects of meiotic inhibitors and gonadotrophins on porcine oocytes in vitro maturation, fertilization and development. Reprod Domest Anim. 52:873–880. https://doi.org/10.1111/RDA.12993

Hamze JG, Cambra JM, Navarro-Serna S, Martinez-Serrano CA. 2025. Navigating gene editing in porcine embryos: methods, challenges, and future perspectives. Genomics. 117:111014. https://doi.org/10.1016/J.YGENO.2025.111014

Hernández-Martínez R, Ramkumar N, Anderson KV. 2019. P120-catenin regulates WNT signaling and EMT in the mouse embryo. Proc Natl Acad Sci U. S. A. 116:16872–16881. https://doi.org/10.1073/PNAS.1902843116/SUPPL_FILE/PNAS.1902843116.SM04.AVI

Huang Y et al. 2013. Moderate expression of Wnt signaling genes is essential for porcine parthenogenetic embryo development. Cell Signal. 25:778–785. https://doi.org/10.1016/J.CELLSIG.2013.01.001

Larasati Y, Boudou C, Koval A, Katanaev VL. 2022. Unlocking the Wnt pathway: therapeutic potential of selective targeting FZD7 in cancer. Drug Discov Today. 27:777–792. https://doi.org/10.1016/J.DRUDIS.2021.12.008

Lin-Schilstra L, Backus G, Snoek H, Mörlein D. 2022. Consumers' view on pork: consumption motives and production preferences in ten European Union and four non-European Union countries. Meat Sci. 187:108736. https://doi.org/10.1016/J.MEATSCI.2022.108736

Liu HY et al. 2024. Frizzled receptors (FZDs) in Wnt signaling: potential therapeutic targets for human cancers. Acta Pharmacol Sin. 45:1556–1570. https://doi.org/10.1038/s41401-024-01270-3

Liu X et al. 2020. Maternal cytokines CXCL12, VEGFA, and WNT5A promote porcine oocyte maturation via MAPK activation and canonical WNT inhibition. Front Cell Dev Biol. 8:547998. https://doi.org/10.3389/FCELL.2020.00578/BIBTEX

Martinez EA et al. 2019. Achievements and future perspectives of embryo transfer technology in pigs. Reprod Domest Anim. 54 Suppl 4:4–13. https://doi.org/10.1111/RDA.13465.

Nusse R, Clevers H. 2017. Wnt/β-catenin signaling, disease, and emerging therapeutic modalities. Cell. 169:985–999. https://doi.org/10.1016/j.cell.2017.05.016

Oldefest M et al. 2015. Secreted frizzled-related protein 3 (sFRP3)-mediated suppression of interleukin-6 receptor release by A disintegrin and metalloprotease 17 (ADAM17) is abrogated in the osteoarthritis-associated rare double variant of sFRP3. Biochem J. 468:507–518. https://doi.org/10.1042/BJ20141231

Peng Y et al. 2025. Structural insights into Wnt/β-catenin signaling regulation by LGR4, R-spondin, and ZNRF3. Nat Commun. 16:8337. https://doi.org/10.1038/s41467-025-64129-z

Pourreyron C et al. 2012. Wnt5a is strongly expressed at the leading edge in non-melanoma skin cancer, forming active gradients, while canonical Wnt signalling is repressed. PLoS One7: e31827. https://doi.org/10.1371/JOURNAL.PONE.0031827

Ranes M, Zaleska M, Sakalas S, Knight R, Guettler S. 2021. Reconstitution of the destruction complex defines roles of AXIN polymers and APC in β-catenin capture, phosphorylation, and ubiquitylation. Mol Cell. 81:3246–3261.e11. https://doi.org/10.1016/J.MOLCEL.2021.07.013

Ren Q, Chen J, Liu Y. 2021. LRP5 and LRP6 in Wnt signaling: similarity and divergence. Front Cell Dev Biol. 9:670960. https://doi.org/10.3389/FCELL.2021.670960

Rogers S, Scholpp S. 2022. Vertebrate Wnt5a – at the crossroads of cellular signalling. Semin Cell Dev Biol. 125:3–10. https://doi.org/10.1016/J.SEMCDB.2021.10.002

Ross C et al. 2025. WNT-mediating TCF/LEF transcription factor gene expression in early human pluripotency and cell lineages differs from the rodent paradigm. J Cell Sci. 138:jcs264257 https://doi.org/10.1242/jcs.264257

Semënov MV et al. 2001. Head inducer dickkopf-1 is a ligand for Wnt coreceptor LRP6. Curr Biol. 11:951–961. https://doi.org/10.1016/S0960-9822(01)00290-1/ASSET/7C87ECC4-B9F5-492C-B82B-1AD4C7057300/MAIN.ASSETS/GR7.JPG

Spate LD et al. 2014. Dickkopf-related protein 1 inhibits the WNT signaling pathway and improves pig oocyte maturation. PLoS One. 9:e95114. https://doi.org/10.1371/JOURNAL.PONE.0095114

Stamos JL, Weis WI. 2013. The β-catenin destruction complex. Cold Spring Harb Perspect Biol. 5: a007898. https://doi.org/10.1101/CSHPERSPECT.A007898

Steinhart Z, Angers S. 2018. Wnt signaling in development and tissue homeostasis. Development. 145: https://doi.org/10.1242/DEV.146589

Tribulo P et al. 2017. WNT regulation of embryonic development likely involves pathways independent of nuclear CTNNB1. Reproduction. 153:405–419. https://doi.org/10.1530/REP-16-0610

Van Der Wal T, Van Amerongen R. 2020. Walking the tight wire between cell adhesion and WNT signalling: a balancing act for β-catenin. Open Biol. 10:200267. https://doi.org/10.1098/RSOB.200267

Zi X et al. 2005. Expression of Frzb/secreted frizzled-related protein 3, a secreted Wnt antagonist, in human androgen-independent prostate cancer PC-3 cells suppresses tumor growth and cellular invasiveness. Cancer Res. 65: 9762–9770. https://doi.org/10.1158/0008-5472.CAN-05-0103

Journal of Animal Science, 2026, 104, 1–13
https://doi.org/10.1093/jas/skag134
Reproduction